JOURNAL OF MATERIALS SCIENCE **40** (2005) 6145–6150

Porous alumina ceramics prepared by slurry infiltration of expanded polystyrene beads

JIANLI LIU, XIGENG MIAO*
School of Materials Science and Engineering, Nanyang Technological University, Nanyang Avenue, 639798, Singapore
E-mail: asxgmiao@ntu.edu.sg

Published online: 8 September 2005

To produce highly porous MgO-doped alumina (Al_2O_3) ceramics, expanded polystyrene (EPS) beads were packed as a pore former and well-dispersed alumina slurry was used to infiltrate the pore space in the EPS bead compacts. The alumina particle-EPS bead green compacts were then heated to 1550°C in air to burn out the pore former and subsequently densify the MgO-doped alumina struts. The porous Al_2O_3 ceramics were featured with uniformly distributed open pore structures with porosities ranging from 72 to 78% and a pore interconnectivity of about 96%. The macropore size and the pore window size could be controlled by adjusting the size of the EPS beads and the contacting area between the EPS beads. The compressive strengths of the porous Al_2O_3 ceramics were in the range of 5.5–7.5 MPa, similar to those of cancellous bones (2–12 MPa). The porous alumina ceramics were further made bioactive after the dip coating of a sol-gel derived 58 S bioglass powder, followed by sintering at 1200°C.

1. Introduction

Tissue engineering has emerged as a potential alternative to the current therapies for tissue reconstruction. Biocompatible porous scaffolds of a metal, a polymer, a bioceramic or a composite are an important component of tissue engineering. Compared with polymers and metals, bioceramics have the advantages of high mechanical strength, high corrosion resistance, excellent biocompatibility, and no swelling or shape distortion after implantation. Therefore, bioceramic scaffolds are particularly important for tissue engineering of bones. Porous bioinert ceramics such as alumina and zirconia are relatively strong but lack bioactivity. Thus it is desirable to produce porous bioinert ceramics that are modified with bioactive coatings consisting of hydroxyapatite, bioglass, or a bioactive glass-ceramic. It is also important to control the porous structural parameters such as porosity, pore size, and pore interconnectivity for bone tissue engineering.

There have been quite a few reported methods for the preparation of porous ceramic scaffolds. Maca *et al*. [1] used carbon particles as a pore former to prepare porous alumina through a dry powder pressing process. Sepulveda *et al*. [2] fabricated porous bioceramics by a foaming method involving in-situ polymerization of a foamed slurry. You *et al*. [3] prepared porous alumina ceramics by coating a cellulose sponge with an alumina slurry, followed by sintering in air. Finally, Bose *et al*. [4] produced alumina scaffolds using polymer scaffolds prepared by fused deposition modeling (FDM), a commercially available rapid prototyping (RP) technique. It should be mentioned that every method for porous bioceramic scaffolds has its own advantages and limitations.

To impart bioactivity to alumina while maintaining the mechanical properties of alumina, HA was coated on highly porous alumina [5]. The compressive strength of the HA coated porous alumina reached 10 MPa, a value ten times higher than that of pure porous HA. Similarly, Jun *et al*. [6] used slurry dipping method to coat porous alumina with HA and tricalcium phosphate (β-TCP). On the other hand, there have been several reports on the coating of dense (not porous) alumina with bioactive glasses and glass-ceramics. Kim *et al*. [7] coated dense alumina with a bioinert glass intermediate layer and a bioactive glass surface layer. Hamadouche *et al*. [8] applied a sol-gel bioactive glass (either 58 S Bioglass or 77 S Bioglass) coating on dense alumina implants. Last but not the least, Verne *et al*. [9] studied a bioactive glass-ceramic coating for modifying a pure and dense alumina substrate. The purpose of this paper is to present a new method to produce porous bioceramics and to report porous alumina ceramics that were modified with the sol-gel derived 58 S bioglass coating.

2. Experimental procedure

Expanded polystyrene beads (BASF Singapore Pte Ltd, Singapore) with particle sizes of 1.4, 2.0 and 2.8 mm

*Author to whom all correspondence should be addressed.
0022-2461
DOI: 10.1007/s10853-005-3165-3

were used as the pore former for the porous alumina. The expanded (or foam-like) polystyrene beads resulted from the usage of pentane as a foaming agent. The morphology of the EPS beads was observed using a scanning electron microscope (SEM, JEOL JSM-5410). The thermal stability of the EPS beads was analyzed using a thermal gravimetric analyzer (Hi-Res TGA 2950 Thermgravimetric Analyzer, TA Instrument).

Commercial α-Al_2O_3 powder (AKP-30, Sumitomo Chemical Co. Ltd, Japan) was used, having a particle size of 0.36 μm and a specific surface area of 6.84 m^2/g. To modify the commercial alumina powder, 0.5 wt% MgO was added using $Mg(NO_3)_2{\cdot}6\ H_2O$ as a precursor, followed by calcination in air at 900°C for 1 h. The calcined and milled MgO-doped alumina (or simply called alumina) powder was used as the starting powder for the study. A 40 wt% ammonium polyacrylate solution (DARVAN® C, R. T. Vanderbilt Company Inc.) was used as the dispersant and a 5 wt% polyvinyl alcohol (PVA) (molecular weight of 72000, Sino Chemical Co. Pte Ltd.) solution was utilized as the binder. In order to prepare an optimized alumina slurry, several alumina suspensions at a solid loading of 60% and with 0, 0.4, 0.6 and 1.0 wt% dispersant (relative to the weight of alumina powder) were prepared. The viscosity of the suspensions was tested using a viscometer (Haake VT500). Before the subsequent slurry infiltration process, 1.5 wt% PVA was added to the optimized alumina slurry, followed by sonication and degassing.

A slurry infiltration apparatus was designed in-house, as shown in Fig. 1. Prior to the casting of the alumina slurry, the expanded polystyrene (EPS) beads were placed in the plastic container and gently pressed by a weight on the cover with holes. The load (or weight) on the EPS bead bed was controlled to obtain a strain or a shrinkage of 15%, which indicated the relative thickness change between the loosely packed and the compressed EPS beads. The alumina slurry was then cast into the container to penetrate the EPS bead bed. A water aspirator was used to create a low vacuum and facilitate the slurry infiltration. After drying, the green compacts consisting of the EPS beads and the alumina particles were heated to 500°C in air at a slow heating rate of 1°C/min to remove the organic species (dispersant, binder and EPS beads), followed by sintering at 1550°C for 2 h to obtain sintered porous alumina ceramics.

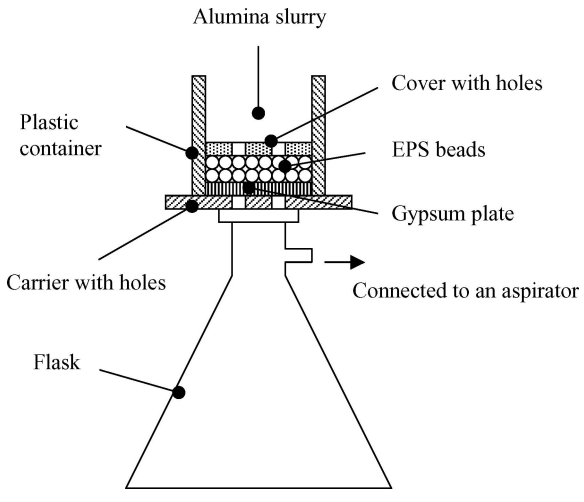

Figure 1 Schematic illustration of the slurry infiltration apparatus.

The porous structures of the as-sintered porous alumina were observed under a stereo-optical microscope (LEICA MZ6) fitted with a digital camera (Olympus DP10). The pore sizes were measured based on the obtained stereo-optical micrographs. The sizes of the small pores (or pore windows) through the macropore walls were also examined under SEM. For porosity measurements and subsequent compressive strength tests, the porous alumina bodies were cut into 20 × 20 × 10 mm specimens using a diamond cutter after the porous alumina bodies were infiltrated with wax. The specimens saturated with wax were weighed to get the saturated weight, W_{sat}. Then the specimens were heated up to 150°C to remove the wax and obtain the net weight, W_{net}. The apparent density (ρ), total porosity (ϕ_t), open porosity (ϕ_o), and pore interconnectivity (p_i) of the porous alumina were then calculated using Equations (1)–(4):

$$\rho = \frac{W_{net}}{V} \tag{1}$$

$$\phi_t = 1 - \frac{\rho}{\rho^*} \tag{2}$$

$$\phi_o = \frac{W_{sat} - W_{net}}{\rho_{wax} V} \tag{3}$$

$$p_i = \frac{\phi_o}{\phi_t} \tag{4}$$

where V is the bulk volume of a porous alumina, ρ^* is the theoretical density of Al_2O_3, i.e., 3.98 g/cm^3, and ρ_{wax} is the theoretical density of wax, i.e., 0.9 g/cm^3. The compressive strengths of the porous alumina were determined using an Instron 4206 tester with a cross-head speed of 0.5 mm/min.

Sol-gel derived 58 S bioglass powder with particle sizes <3 μm and a composition of 58 mol% SiO_2-38 mol% CaO-4 mol% P_2O_5, was used for the bioglass coating. The bioglass powder was prepared through the hydrolysis and condensation of a mixed solution of tetraethoxysilane (TEOS, $Si(OC_2H_5)_4$), triethylphosphate (TEP, $OP(OC_2H_5)_3$) and calcium nitrate tetrahydrate ($Ca(NO_3)_2{\cdot}4H_2O$) with HCl as a catalyst [10]. Dried 58 S bioglass gel was then calcined at 700°C for 2 h, followed by ball milling to obtain the 58 S bioglass powder. Then aqueous bioglass slurry with 50 wt% solid loading and 3 wt% PVA binder (relative to the weight of bioglass powder) was prepared to coat the porous alumina through a slurry dipping method. The bioglass slurry-coated porous alumina was then dried and sintered in air at 1200°C for 1 h. The fracture surface of the bioglass coated porous alumina was examined under SEM.

3. Results and discussion

3.1. Characteristics of EPS beads

In the present study, the EPS beads were packed to form an EPS bead bed with the pore space to be infiltrated by the alumina slurry. The geometry of the pore space was determined by the shape, size, and size distribution of the EPS beads, as well as the surface morphology of the EPS beads. Thus the geometry of the strut network of the porous alumina was controlled by the geometry of the pore space in the EPS bead bed. For instance, the surface roughness of EPS beads would determine the surface roughness of the pore walls of the final porous alumina. Fig. 2 shows that the EPS bead had a rather rough surface. Micropores of 1-2 μm in size and macropores larger than 20 μm were present. In Fig. 2, a network of pore-free paths is also observed. Our SEM observation did reveal that the pore wall surfaces of the porous alumina resembled surface morphologies of the EPS beads.

Fig. 3 shows the curves of the weight loss of the EPS beads versus the temperature, measured at different heating rates: 1, 2, 5, and 10°C/min. It can be seen that the EPS beads could be completely burnt out below 500°C. It can also be seen that a lower heating rate corresponded to a lower temperature at which the EPS beads could be burnt out completely. The majority of the weight loss occurred from 350 to 450°C. Below 350°C, the EPS beads experienced thermal expansion with a thermal expansion coefficient of 35 $\times$ 10^{-6} °C^{-1} (given by the manufacturer), in contrast to the value of 90–150 $\times$ 10^{-6}°C^{-1} of unexpanded (or dense) polystyrene (PS) beads. The thermal behavior of the EPS beads had an effect on the integrity of the porous alumina. From a green compact containing the alumina particles and the EPS beads to the state of complete removal of the EPS beads, the porous network of the packed alumina particles was still very weak due to the lack of binding or necking of the alumina particles. Thus, it was important to maintain the integrity of the network of the packed alumina particles. In this regard, the EPS beads were advantageous due to their low thermal expansion coefficient as compared to the dense PS beads. As the thermal expansion coefficient of the EPS beads was low, the stresses experienced by the alumina particle networks due to the thermal expansion of the EPS beads should also be low. Finally, a slow heating rate was desirable for avoiding the rapid thermal expansion of the EPS beads and removing the EPS beads through slow burning and thus could reduce the stress transmitted to the alumina network.

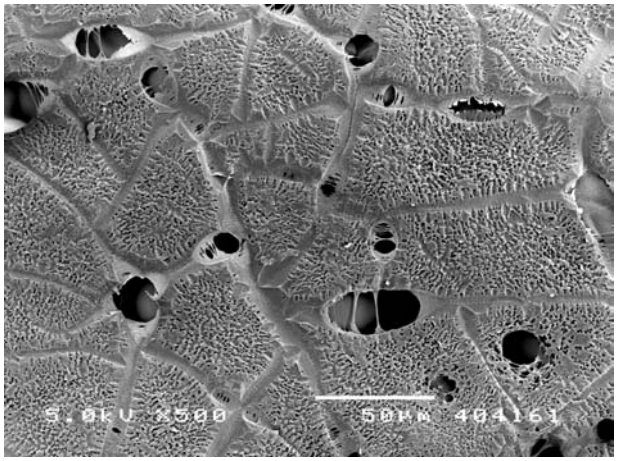

Figure 2 SEM micrograph showing the surface morphology of the EPS bead.

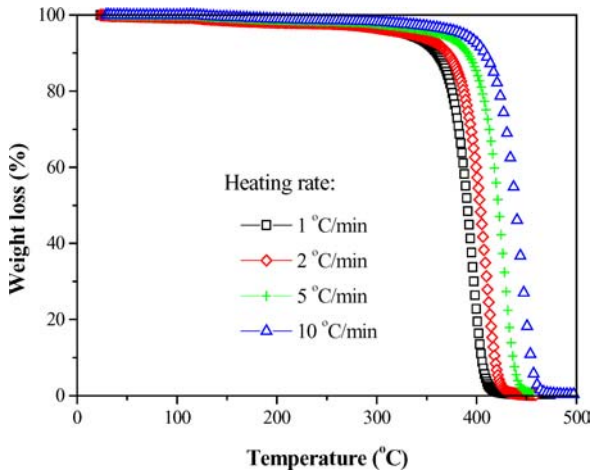

Figure 3 TGA curves of the EPS beads measured at different heating rates: 1, 2, 5, and 10°C/min.

3.2. Flowability of the aqueous alumina slurry

In the present preparation method, the alumina slurry was required to have a good flowability so that the pore space among the EPS bead bed could be completely infiltrated. Fig. 4 shows the viscosities of the alumina suspensions with a solid loading of 60 wt% and having different dispersant contents versus the shear rate. It can be seen that all the suspensions with the dispersant exhibited a shear-thickening behavior, whereas the suspension without the dispersant showed a shear-thinning behavior in the lower shear rate range (0–380 s^{-1}). Fig. 4 also shows that the dispersant addition decreased the viscosity and improved the flowability of the suspensions. With 0.4 to 0.6 wt% dispersant, the viscosities of the suspensions were pronouncedly decreased compared with the dispersant-free suspension. Further addition of the dispersant however slightly increased

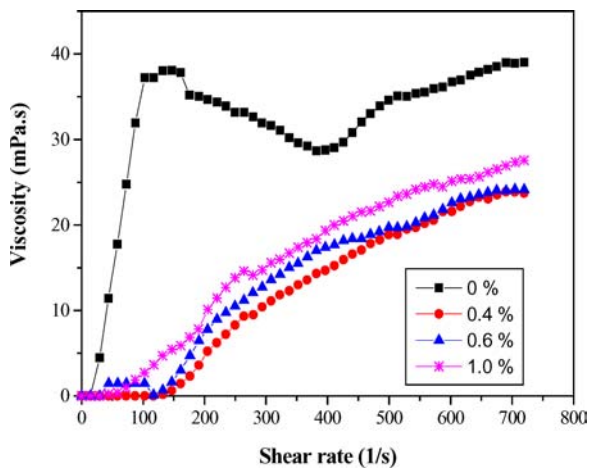

Figure 4 Flow curves of alumina suspensions at a solid loading of 60 wt% and with different dispersant contents.

the viscosities. Therefore, the well-dispersed suspension was obtained with about 0.5 wt% dispersant. The well-dispersed alumina slurry resulted in dense alumina particle packing (about 55% theoretical density) in the pore space among the EPS bead bed and also resulted in small sintering shrinkage (~15%) of the porous alumina. The dense particle packing and the low sintering shrinkage were important for achieving the integrity of the obtained porous alumina.

3.3. Structural characteristics of the porous alumina ceramics

Fig. 5 shows a stereo-optical micrograph of the porous alumina prepared using EPS beads with the particle size of about 2 mm and with a strain of 15% applied on the EPS bead bed. It can be seen that the macropores were uniformly distributed with an average pore size about 1.6 mm and nearly all the macropores were interconnected. Fig. 6 is an SEM micrograph from the same sample as for Fig. 5. It can be seen that the struts had the narrowest regions with a thickness about 200 μm. The openings or windows through the macropore walls had average diameter about 500 μm. These pore windows were large enough for bone ingrowth, since various studies have indicated the minimal pore sizes of 150 – 200 μm for bone ingrowth. The struts of the porous alumina produced in the present study were more bulky or contained more solid alumina as compared to those of typical porous alumina prepared by polyurethane foam dipping method. The struts of the porous alumina produced currently also had no hole-like defect, as in the case of porous alumina prepared from the polyurethane foam dipping method.

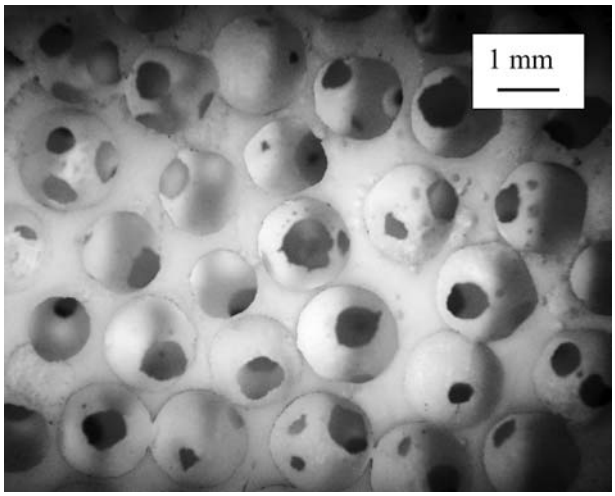

Figure 5 Stereo-optical micrograph showing an overall porous structure of a porous alumina prepared using the EPS beads of 2.0 mm in size and compressed with the strain of 15%.

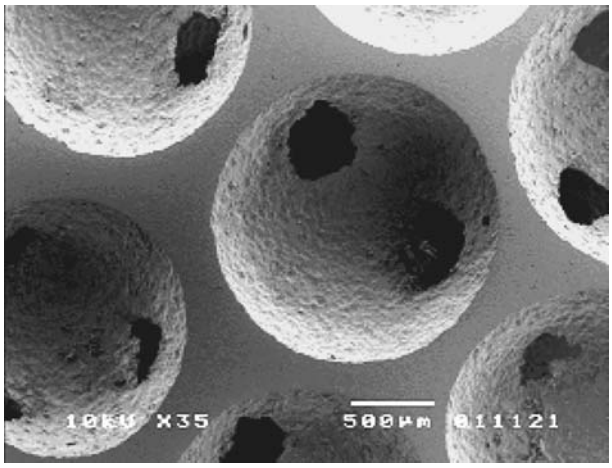

Figure 6 SEM micrograph showing the pore windows in the macropores and the solid struts of the porous alumina prepared using EPS beads of 2.0 mm in size and compressed with the strain of 15%.

TABLE I Some structural parameters of the porous alumina ceramics

Sample	Size of EPS beads (mm)	Pore size (mm)	Pore window size (μm)	Total porosity (%)	Open porosity (%)	Pore interconnectivity (%)
A	1.4	1.1	450	72.5	69.2	95.5
B	2.0	1.6	500	76.9	74.2	96.5
C	2.8	2.0	600	78.1	75.8	97.1

Table I summarizes the structural characteristics of the porous alumina ceramics prepared in the current study. It can be seen that the pore sizes of the macropores were smaller than the sizes of the original EPS beads used. This was because that solid state sintering of the α-Al_2O_3 particles resulted in sintering shrinkage of the strut networks and thus the reduction of the macropore sizes. When the sintering condition was kept the same, larger EPS bead sizes resulted in larger pore sizes of the porous alumina ceramics. The pore interconnectivity levels were also high and comparable to those commonly achieved using the polyurethane foam dipping method. However, the total porosities (72.5 to 78.1%) were lower than those of porous ceramics typically achieved in the polyurethane foam dipping method.

The pore structures of the porous alumina ceramics could be effectively controlled by the packing conditions of the EPS beads. Apart from the factors of shape, size, size distribution, and surface morphology of the EPS beads, another important factor was the contacting pressure between the EPS beads, as controlled by the strain of the EPS bead bed used in the study. If no pressure was applied on the EPS bead bed, the alumina slurry and the resultant alumina green compact tended to isolate the EPS beads and resulted in closed porosity. If too much pressure was used, the pore space among the EPS bead bed became too small for slurry infiltration, which affected the infiltration efficiency and also the strut thickness of the final porous alumina.

3.4. Mechanical strength of the porous alumina ceramics

Fig. 7 shows the compressive strengths of the porous alumina ceramics prepared using EPS beads of different sizes. The compressive strengths ranging from 7.5 to 5.5 MPa were comparable to those of cancellous bones, ranging from 2 to 12 MPa. Such high compressive strengths for such high porosities (71.5–78.1%)

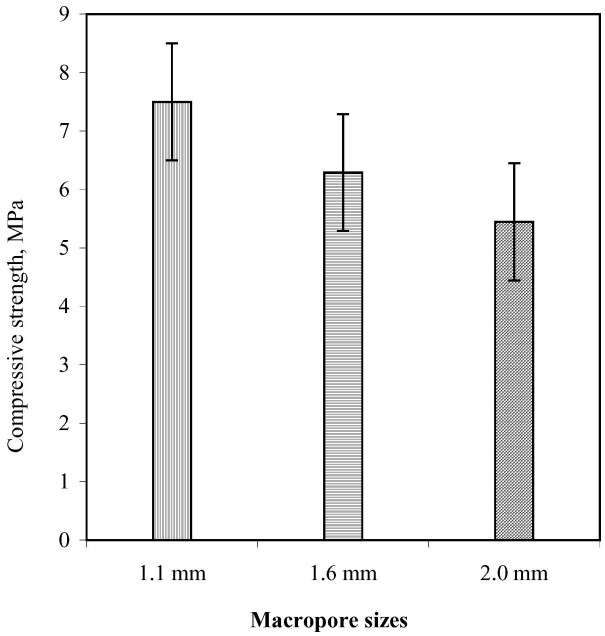

Figure 7 The compressive strengths of the porous alumina ceramics prepared using EPS beads of different sizes.

were related to the nature of alumina ceramics and the microstructure of the alumina struts. Fig. 8 shows the fracture surface of a alumina strut of the porous alumina. It can be seen that the microstructure was featured with relatively uniform grains around 3 μm in size. Nearly no residual pores existed inside the alumina grains. Such a microstructure was due to the addition of 0.5 wt% MgO, since our observation on pure alumina ceramics revealed many residual pores trapped in the grains, which were not uniform with some as large as 15 μm. It should be noted that the effect of MgO on alumina in terms of densification and grain size control was known long time ago [11]. It should also be noted that higher compressive strengths would be possible if the current processing parameters were optimized further and if yttria-stabilized zirconia particles were introduced as a second phase in the struts.

Furthermore, from Table I and Fig. 7, one can see that the compressive strength of the porous alumina ceramics decreased with the increase of the total porosity. Since the struts had very few micropores, the total porosity should be due to the presence of the macropores. Since the open porosity was only slightly smaller than the total porosity, some macropores could be closed or without windows through the macropores. Thus, the compressive strength actually decreased with the open porosity, which could be explained by the well-known Gibson-Ashby model [12]. According to the model, the compressive strength of a highly porous structure, σ_c, is related to the bending strength of the struts, σ_{f0}, and the open macroporosity, ϕ, of the porous structure:

$$\sigma_c = k\sigma_{f0}(1-\varphi)^{3/2} \quad (5)$$

where k is a constant. Thus one can see that Equation (5) predicts the decrease of the compressive strength with the increase of the open macroporosity.

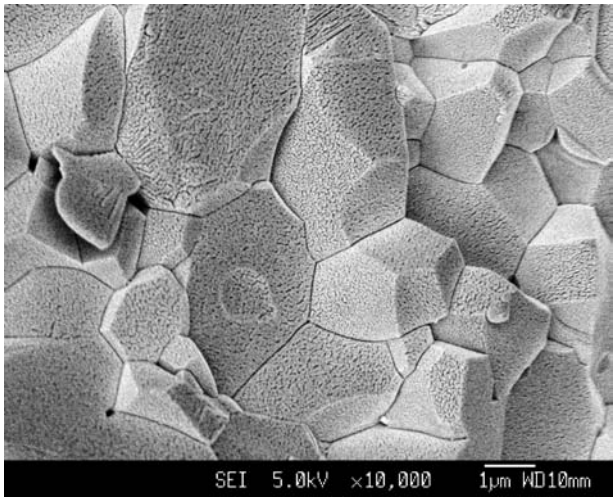

Figure 8 SEM micrograph showing the fracture surface of a strut of the porous alumina.

3.5. Bonding of bioglass coating on porous alumina

Fig. 9 shows the fracture surface of the bioglass-coated porous alumina. It can be seen that the fracture occurred across the alumina substrate and the bioglass coating instead of along the interface between the substrate and the coating, which indicated the strong bonding of the 5–9 μm thick bioglass coating. In our previous work [13], the thermal expansion coefficients (CTEs) of the 58S bioglass and the alumina ceramics were measured as $0.73\times10^{-6}/^{\circ}$C and $9.47\times10^{-6}/^{\circ}$C, respectively. Due to the smaller CTE of the bioglass compared to that of alumina, the residual thermal stresses in the bioglass coating as a result of the cooling process should be compressive rather than tensile in nature. This compressive nature of the residual thermal stresses can be understood by considering a simple model of a bioglass layer on a large alumina plate. During the cooling period and starting from the softening temperature of the bioglass (~600 C), the faster shrinking alumina substrate would hold and push the bioglass layer towards the planar center of the bioglass layer, causing a compressive stress in the bioglass layer and parallel to the interface. Qualitative analysis of the residual stresses can be found in literature. Briefly, the level of a residual thermal stress is dependent on parameters such as the Young's moduli of the individual components, the thermal expansion coefficient mismatch, the thickness ratio and the temperature change during the cooling process. In the current situation, although the CTEs were quite different between the substrate and the coating, the residual compressive stresses in the bioglass coating could be still small due to its small thickness, low Young's modulus, and low softening temperature (~600°C). The compressive nature and the low level of the residual stresses discussed above should be considered as desirable in terms of cracking prevention. Indeed, no cracking within the bioglass coating and no delamination across the interface were observed, indicating the good interfacial bonding. In addition to the high mechanical integrity, the 58 S bioglass coating was confirmed to be bioactive in our other studies [13], although the so-called bioglass was actually a bioactive

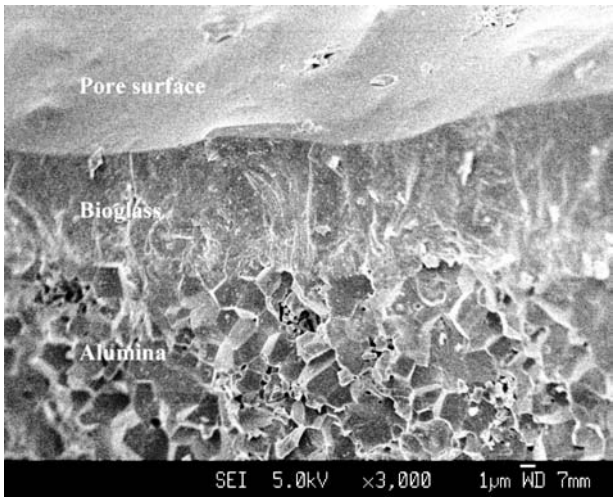

Figure 9 SEM micrograph showing the fracture surface of a bioglass-coated alumina strut.

glass-ceramic with a $CaSiO_3$ phase (β-wollastonite) being detected. The currently obtained porous alumina ceramics with the bioglass coating would be a potential biomaterial due to the high mechanical strength and the bioactivity.

4. Conclusion

Porous MgO-doped alumina ceramics with well-interconnected porous structures were fabricated using the expanded polystyrene (EPS) bead compacts as the pore former and via the infiltration of well-dispersed alumina slurry, followed by firing at 1550°C in air. The open porosity and the average pore size of the porous alumina could be controlled by adjusting the size of the EPS beads. The size of the pore windows could also be adjusted by using a proper pressure on the compressible EPS beads with 450 to 600°μm being obtained in the current experimental conditions. The open porosity, the pore size, and the pore interconnectivity were 69–76%, 1.1–2 mm and around 96%, respectively. The compressive strengths of the porous alumina ceramics ranged from 5.5 to 7.5 MPa, which were close to those of cancellous bones (2–12 MPa). These findings suggested that the method of slurry infiltration of EPS bead compacts was feasible to fabricate porous alumina ceramics. Furthermore, a bioactive 58 S bioglass layer (12–15 μm) was successfully coated on the porous MgO-doped alumina, resulting in a desirable combination of both high mechanical strength and good bioactivity.

Acknowledgment

The authors would like to acknowledge the financial support of the Nanyang Technological University in Singapore (AcRF RG26/01).

References

1. K. MACA, P. DOBSAK and A. R. BOCCACCINI, *Ceram. Int.* **27** (2001) 577.
2. P. SEPULVEDA, *Am. Ceram. Soc. Bulletin* **76** (1997) 61.
3. C. K. YOU, S. H. OH, J. W. KIN, T. H. CHOI, S. Y. LEE and S. Y. K. KIM, *Key Eng. Mater.* **240/242** (2003) 563.
4. S. BOSE, J. DARSELL, H. L. HOSICK, L. H. YANG, D. K. SARKAR and A. BANDYOPADHYAY, *J. Mater. Sci. Mater. Med.* **13** (2002) 23.
5. G. W. JIANG and D. L. SHI, *J. Biomed. Mater. Res.* **43** (1998) 77.
6. Y. K. JUN, W. H. KIM, O. K. KWEON and S. H. HONG, *Biomaterials* **24** (2003) 3731.
7. C. Y. KIM and S. S. JEE, *J. Euro. Ceram. Soc.* **23** (2003) 1803.
8. M. HAMADOUCHE, A. MEUNIER, D. C. GREENSPAN, C. BLANCHAT, J. P. ZHONG, T. G. P. LA and L. SEDAL, *Key Eng. Mater.* **192/195** (2001) 413.
9. E. VERNE, C. V. BROVARON, C. MOISESCU, E. GHISOLFI and E. MARMO, *Acta Mater.* **48** (2000) 4667.
10. J. P. ZHONG and D. C. GREENSPAN, *J. Biomed. Mater. Res.* **53** (2000) 694.
11. J. C. RICHARD, P. SVANTE and E. S. CURTIS, US Patent No. 4285732, 1981.
12. L. J. GIBSON and M. F. ASHBY, in Cellular Solids: Structure and Properties. (Cambridge University Press, Cambridge, 1997) p. 20.
13. J. LIU and X. MIAO, *Ceram. Int.* **30** (2004) 1781.

Received 21 May 2004
and accepted 6 May 2005